J Nanostruct 14(3): 845-856, Summer 2024

RESEARCH PAPER

Isotherm and Thermodynamic Analysis of Azur C Dye Adsorption on GO/P(CMC-Co-Am) Nanocomposite

Alzayd Asawer A. Mhammed [1], Amna N. Zghair [2], Ali M. Essa [3], Ahmed Salim jawad [4], May Jaleel Abed [3], Maryam Batool [5], and Layth S. Jasim [3] *

[1] *Branch of Physiology, Biochemistry and Pharmacology, College of Veterinary, University of Kerbala, Kerbala, Iraq*

[2] *Ministry of Education General Directorate of Al-Qadisiyah Education, Diwaniyah, Iraq*

[3] *Department of Chemistry, College of Education, University of Al-Qadisiyah, Diwaniyah, Iraq*

[4] *College of Veterinary, University of Kerbala, Kerbala, Iraq*

[5] *Department of Chemistry, University of Sahiwal, Sahiwal, Pakistan*

ARTICLE INFO

Article History:
Received 23 March 2024
Accepted 19 June 2024
Published 01 July 2024

Keywords:
Azure C
GO/P(CMC-Co-Am) nanocomposite
Isotherms
Thermodynamic study
Water treatment

ABSTRACT

Water pollution is one of the critical challenges of today's society. Dyes are carcinogenic pollutants that are resistant to degradation and their adsorptive removal from water require some adsorbents with higher adsorption efficiency. Current research focuses on the adsorptive removal of Azure C dye onto a graphene oxide-carboxymethyl cellulose-co-acrylamide (GO/P(CMC-Co-Am)) nanocomposite synthesized via free radical copolymerization process. Batch adsorption study was carried out for bitter understanding the effects of dye concentration and temperature on adsorption efficiency. Data from concentration study and temperature was applied to different isotherm models and thermodynamic study. Results revealed that Freundlich isotherm model fits best to adsorption data (R^2 = 0.9219), highlighting the heterogeneous adsorption. Furthermore, high temperature results in decreasing the adsorption capacity, revealing the exothermic nature of the adsorption process. Thermodynamically, the process was spontaneous and exothermic in nature with a decrease in entropy over a range of temperature. Overall, results showed the effectiveness of GO/P(CMC-Co-Am) nanocomposite for adsorption of Azure C dye from water.

How to cite this article
Mhammed A., Zghair A., Essa A., jawad A., Abed M., Batool M., Jasim L. Isotherm and Thermodynamic Analysis of Azur C Dye Adsorption on GO/P(CMC-Co-Am) Nanocomposite. J Nanostruct, 2024; 14(3):845-856. DOI: 10.22052/JNS.2024.03.015

INTRODUCTION

One of the major contributors of pollutants discharge into the water system is textile industry [1, 2] that generally contains variety of compounds, dyes, ions, salts, and other organic and inorganic substances. According to an estimation, textile industry is responsible for discharge of nearly 100 tons of dyes in water per annum [3]. The excessive release of dyes into water system results in environmental pollution thereby affecting all life forms of it. Among the variety of pollutants in water, dyes are the common pollutants present in large amount. One of the most common dyes is cationic Azure C dye that was conventionally used for dying fabrics such as silk, leather, and paper. The solubility of this dye is high in water and its

* *Corresponding Author Email: layth.alhayder@gmail.com*

maximum absorbance take place at the wavelength (λmax) of 611.5 nm. The chemical formula of dye is $C_{13}H_{12}ClN_3S$, and is commonly known as Basic Violet 3 [4]. Azure C dye when present in very high concentrations in water it resulted in affecting both aquatic and terrestrial life [5]. This led to the need for treating dye loaded water using some effective wastewater treatment technologies [6-12]. Nowadays, researchers put their utmost efforts in treating polluted water using some promising methods that include physical, chemical and some biological methods [13-15]. Among all previously mentioned techniques, adsorption technique is one of the widely employed method for water treatment and has been used earlier by many researchers [16-18]. The simple design, effectiveness, and cost-efficient nature of this process make this a promising technique for treating water containing variety of pollutants [19]. Till yet, variety of adsorbents studied and employed for adsorption of dyes from water [20-30].

Adsorption is a process where in a material transition from a liquid phase to a solid surface, establishing chemical and/ or physical interactions. Various types of sorbents are utilized in these processes, contributing to the complex phenomenon of retaining metal ions and organic ligands in soil [19, 31]. Hydrogels, characterized as three-dimensional polymeric networks with high porosity, can absorb and retain substantial quantities of water when swollen, thereby showing great potential as adsorbents for metals [32]. The literature review indicates that the FTIR technique is employed to analyze the functional groups present on hydrogel surfaces. Common functional groups identified on biocarbon surfaces include C=C, C=O, O–H, C–O, O–CH_3, and C–H. These functional groups are believed to facilitate the adsorption of dyes [33, 34], Sodium alginate (SA), chitosan, cellulose, and lignin [35] are natural polysaccharides that are generally low-cost and readily available [36]. Given its excellent biocompatibility and biodegradability, sodium alginate is considered an ideal bio-adsorbent substrate. Research has demonstrated that SA can effectively remove toxic heavy dyes, such as cationic Azure C dye [37], Graphene oxide (GO) is a biocompatible and non-toxic material that demonstrates excellent performance even at low concentrations [38]. GO contains various functional groups, including hydroxyl, carboxyl, and epoxy groups, on both its interior and surface, allowing it to degrade toxic pollutants through mechanisms such as electrostatic interaction, chemical reactions, and hydrogen bonding [39]. Additionally, GO features a high specific surface area and an abundance of surface functional groups. This study, therefore, aimed at adsorption of Azure C dye using nanocomposite material synthesized by free radical copolymerization of graphene oxide and carboxymethyl cellulose-co-acrylamide (GO/P(CMC-Co-Am)). Furthermore, the research aimed to understand the thermodynamics and isothermal modeling of the dye adsorption process, providing valuable insights into the factors affecting adsorption.

MATERIALS AND METHODS

Materials and chemicals used

The chemicals used in study were sodium chloride, potassium chloride, calcium chloride, potassium persulfate, bis-acrylamide, acrylamide, carboxymethyl cellulose sodium salt, nitrogen gas, graphite (5µm), hydrochloric acid, sodium nitrate, potassium permanganate, hydrogen peroxide and

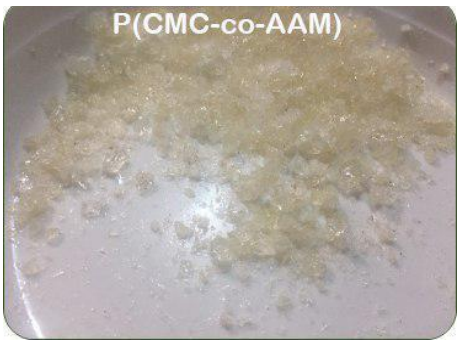

Fig. 1. Prepared hydrogel P(CMC-Co-Am).

barium chloride.

Synthesis of hydrogel P(CMC-Co-Am)

The hydrogel i.e., P(CMC-Co-Am) was synthesized by the process of free radical copolymerization. For this, 0.05 g sodium carboxymethyl cellulose (CMC) was dissolved in 50 mL deionized water. Subsequently, 12 grams of acrylamide was gradually added to the solution, which was placed in a three-necked round-bottom flask equipped with a condenser, a separatory funnel, and a nitrogen gas inlet. The mixture was stirred until complete dissolution, then 0.18 grams of N, N'-methylenebisacrylamide (MBA) was incorporated, followed by two drops of TAMAD and 0.12 grams of potassium persulfate (KPS) as the initiator. Each component was added sequentially under a nitrogen atmosphere with continuous stirring for two hours at 60 degrees Celsius. Upon completion, the resulting hydrogel was cut into small pieces and washed thoroughly with deionized water under constant stirring for six hours, replacing the water every 30 minutes to remove any unreacted materials. Finally, the hydrogel was dried in an oven at 60 degrees Celsius until it reached a constant weight (Fig. 1).

Synthesis of GO/P(CMC-Co-Am) nanocomposite

The polymer nanocomposite hydrogel was synthesized using free radical copolymerization in an aqueous solution. Sodium carboxymethyl cellulose (CMC) was dissolved in deionized water, followed by the gradual addition of acrylamide. The resulting solution was placed in a three-necked round-bottom flask equipped with a condenser, a separatory funnel, and a nitrogen gas inlet. After its complete stirring, pre-dissolved graphene oxide (GO) added to above mixture with the help of separatory funnel. This was followed by adding potassium persulfate (KPS, initiator) to mixture with constant stirring under nitrogen at 60°C for 2 hours. The resulting obtained polymer nanocomposite hydrogel was then cut into smaller pieces that were washed thoroughly with water for removing unreacted materials. Afterwards, hydrogel was oven-dried at 60°C till a constant weight was obtained (Fig. 2).

Characterization of adsorbent

For the identification of different functional groups of adsorbents, Fourier Transform Infrared (FTIR) analysis was carried out (Shimadzu 8400s spectrophotometer) within range of 500 to 4000 cm^{-1} [7, 40, 41]. Additionally, the surface analysis of adsorbents was studied with the help of Field Emission Scanning Electron Microscopy (FESEM) (TESCAN MIRA3) using an accelerating voltage of 25 kV that provides information regarding surface structure and morphology of adsorbents, which can influence their adsorption properties [42]. X-ray Diffraction (XRD) analysis was also carried out (Shimadzu XRD-6000) for analysis of crystal structure and crystallinity of adsorbents with 2θ range of 10° to 80° [43, 44].

Adsorption study

To investigate the influence of dye concentration and temperature on the adsorption of Azure C dye by the GO/P(CMC-Co-Am) nanocomposite, batch adsorption experiments were conducted under controlled conditions. Temperature was varied between 10°C and 30°C while maintaining constant initial dye concentrations (10-100 ppm), contact time (120 minutes), shaking speed (130

Fig. 2. Prepared GO/P(CMC-Co-Am) nanocomposite.

rpm), pH (7.0), and adsorbent dose (0.1 g). The adsorption efficiency was evaluated at different temperatures to assess the impact of temperature on the adsorption process in terms of adsorption capacity that was calculated by using Eq. 1:

$$q_e = \frac{C_0 - C_e}{M} \times V \quad (1)$$

here C_0 and C_e refers to initial and equilibrium dye concentrations (mg/l), V and M refers to volume (mL) of solution and adsorbent weight (g) used, correspondingly.

The experimental data were analyzed using various isotherm models (e.g., Langmuir, Freundlich and Temkin) to elucidate the adsorption mechanism. The Langmuir model assumes monolayer adsorption on adsorbent surface [7] while Freundlich model deals with multilayer adsorption [16]. Temkin model concerned with adsorbent-adsorbate interactions and heat of adsorption variation [45]. Linear equations used for Langmuir, Freundlich and Temkin model are given in Eqs. 2, 3 and 4 respectively.

$$\frac{1}{q_e} = \frac{1}{q_{max}} + \frac{1}{q_o b C_e} \quad (2)$$

where b (L/mg) and q_{max} (mg/g) denotes Langmuir constant and maximum adsorption capacity correspondingly.

$$\frac{1}{q_e} = \frac{1}{q_{max}} + \frac{1}{q_o b C_e} \quad (3)$$

where k_f and n refers to Freundlich constant (mg/g) and exponent, correspondingly [56].

$$q_{eq} = B \ln A_T + B \ln C_{eq} \quad (4)$$

here, R is universal gas constant (J/mol K), B is constant associated with adsorption heat (J/mol), A_T, b_T and T represents constant of Temkin equilibrium binding (L/ g), Temkin constant (J/mol) and absolute temperature (K) respectively [45].

Additionally, to investigate the adsorption mechanism and thermodynamics of the process, thermodynamic parameters (ΔH, ΔS, and ΔG) were calculated. The distribution coefficient (Kc) was used to determine ΔG. The slope and intercept of a plot of ln(Kc) versus 1/T were used to calculate ΔH and ΔS. These parameters provide insights into the spontaneity, feasibility, and nature of the adsorption process. For calculation of ΔG (Eq. 5),

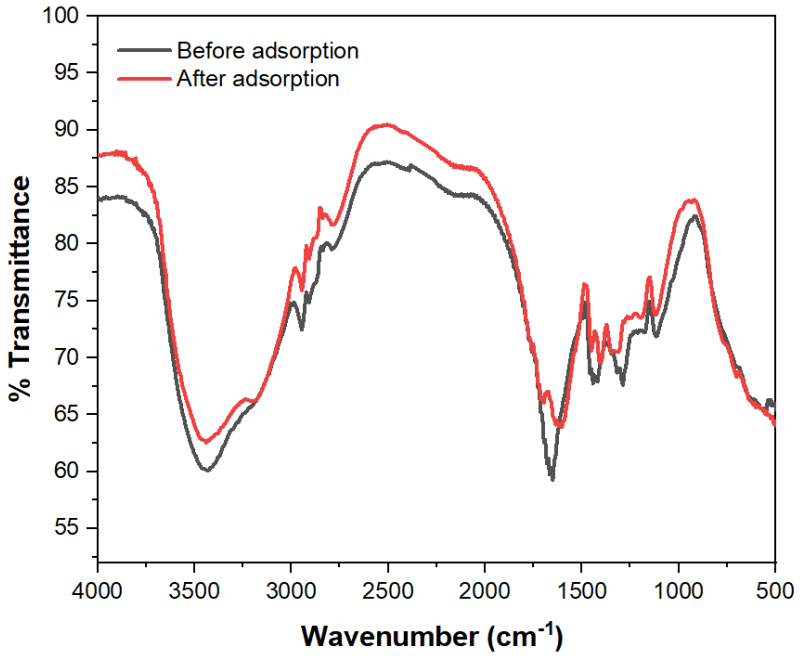

Fig. 3. FTIR of prepared GO/P(CMC-Co-Am) nanocomposite both before and after Azure C dye adsorption.

value of distribution coefficient, k_c, was used (Eq. 6):

$$\Delta G = -RT \ln k_c \quad (5)$$

$$k_c = \frac{C_{ad}}{C_e} \quad (6)$$

where C_{ad} (mg/L), R and T is adsorbed dye concentration, gas constant (8.314 J/mol K) and absolute temperature (K), respectively. The Gibbs free energy change (ΔG) can be calculated using the Eq. 7:

$$\Delta G = \Delta H - T\Delta S \quad (7)$$

Substituting Eq. 5 into Eq. 7, an equation of $\ln k_c$ can be obtained as shown in Eq. 8:

$$\ln k_c = -\frac{\Delta H}{RT} + \frac{\Delta S}{R} \quad (8)$$

By plotting a graph of ln(Kc) versus 1/T, the enthalpy change (ΔH) and entropy change (ΔS) can be determined from the slope and intercept, respectively.

RESULTS AND DISCUSSION

FTIR study

The FTIR spectrum of the GO/P(CMC-Co-Am) nanocomposite before adsorption (Fig. 3, black line) exhibits several prominent peaks associated with functional groups. A broad peak at approximately 3400 cm^{-1} indicates the presence of hydroxyl (-OH) stretching, likely originating from carboxyl and hydroxyl groups on graphene oxide (GO) and the polymeric components (CMC and P(CMC-Co-Am)). The peak near 1700 cm^{-1} corresponds to carbonyl (C=O) stretching, possibly from carboxyl groups on GO or amide functionalities in the nanocomposite. Additionally, a peak around 1600 cm^{-1} is attributed to C=C stretching from the aromatic rings of graphene oxide. In the lower wavenumber region (1000-1500 cm^{-1}), peaks arise due to C-O and C-N stretching, as well as other vibrational modes characteristic of the polymer backbone and oxygenated groups within the nanocomposite. Following the adsorption of Azure C dye (Fig. 3, red line), the FTIR spectrum reveals several notable changes. The intensity of the 3400 cm^{-1} peak associated with hydroxyl (-OH) stretching decreases, suggesting the involvement of these

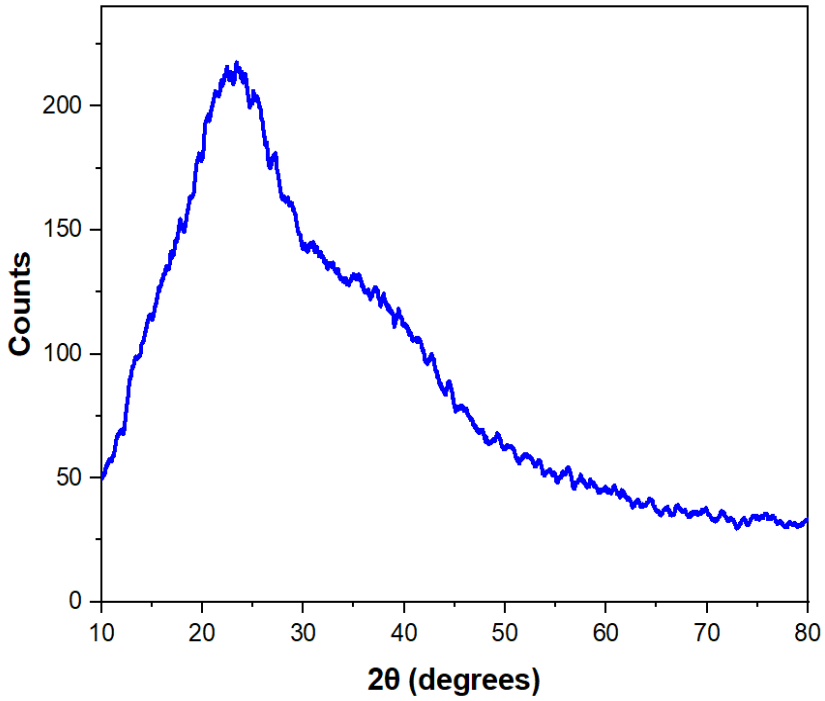

Fig. 4. XRD of prepared GO/P(CMC-Co-Am) nanocomposite.

groups in interactions with the dye, possibly through hydrogen bonding. The peak near 1700 cm^{-1} for carbonyl (C=O) stretching also exhibits slight shifts, indicating potential interactions with dye molecules, potentially via electron interactions or hydrogen bonding. The 1600 cm^{-1} peak for C=C stretching shows minor changes, suggesting π-π stacking interactions between the aromatic rings of the dye and graphene oxide. In the fingerprint region (1000-1500 cm^{-1}), several peaks undergo changes in intensity or shift slightly, indicating the participation of various functional groups, such as C-O and C-N, in the adsorption process, reflecting the complex interactions between the dye molecules and the nanocomposite surface [4, 46-51].

XRD study

The XRD pattern of the GO/P(CMC-Co-Am) nanocomposite (Fig. 4) exhibits a broad peak centered around 2θ of 20-30°, indicative of an amorphous or semi-crystalline structure. This broad peak suggests the presence of disordered graphene oxide (GO) sheets, possibly due to exfoliation or interactions with the polymer matrix, which disrupt the regular stacking of GO layers. The lack of sharp peaks at higher angles confirms the limited crystallinity of the nanocomposite, with the polymer contributing to its overall amorphous nature. This pattern indicates the successful integration of GO into the polymer matrix [52].

FESEM study

The FESEM images of the prepared GO/P(CMC-Co-Am) nanocomposite before dye adsorption (Fig. 5a) exhibit a rough and porous surface morphology, which is favorable for adsorption applications. Images captured at various magnifications reveal clusters of irregularly shaped particles in the nanometer range (approximately

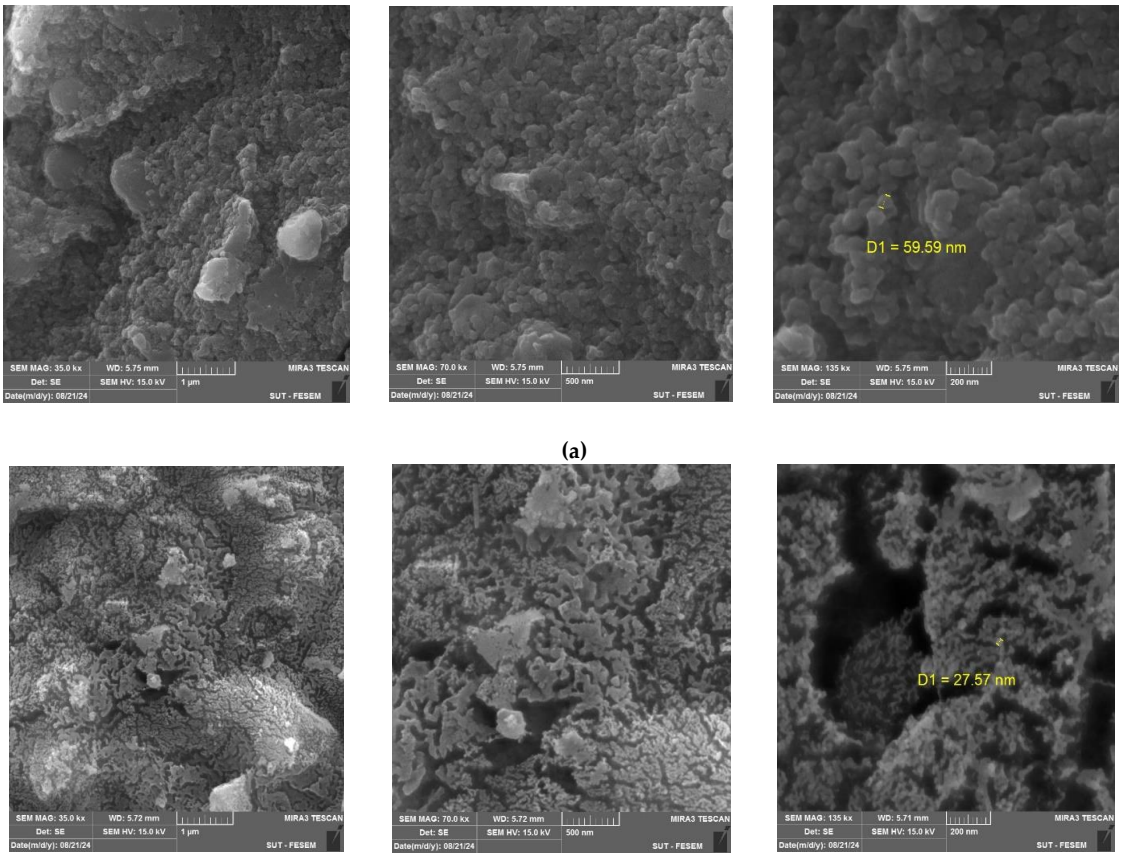

(a)

(b)

Fig. 5. FESEM of prepared GO/P(CMC-Co-Am) nanocomposite both (a) before and (b) after Azure C dye adsorption.

59.59 nm). The porous structure, characterized by noticeable agglomerates, suggests a high surface area, which is advantageous for facilitating dye adsorption. The nanoscale features and porosity observed indicate that the nanocomposite possesses a well-developed surface, suitable for effective interaction with dye molecules during the adsorption process [53]. The FESEM images of the GO/P(CMC-Co-Am) nanocomposite after adsorption (Fig. 5b) reveal significant changes in surface morphology compared to the raw nanocomposite. The previously observed rough and porous surface appears partially covered or filled, suggesting that dye adsorption has occurred both on the surface and within the pores of the nanocomposite. The post-adsorption images exhibit a more compact structure with reduced pore visibility, indicating that dye molecules have occupied the available surface area, leading to decreased porosity (approximately 27.87 nm), possibly indicating aggregation of dye molecules or changes in particle dimensions due to adsorption. Overall, results confirm successful adsorption, characterized by clear surface modifications

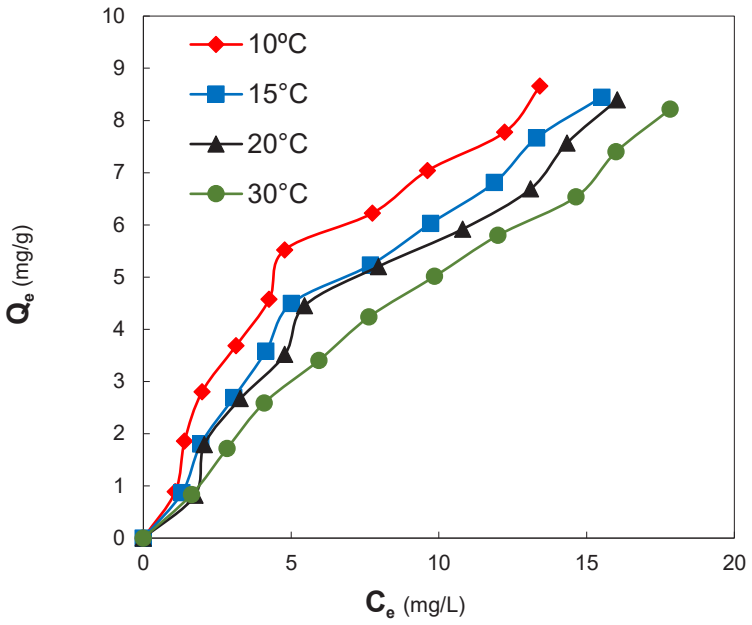

Fig. 6. Adsorption of Azure C dye onto prepared GO/P(CMC-Co-Am) nanocomposite at variable temperatures.

Table 1. Effect of dye concentration on Azure C dye removal at variable temperatures.

	10 °C		15 °C		20 °C		30 °C	
C_o (mg/L)	C_e (mg/L)	q_e (mg/g)	C_e (mg/L)	q_e (mg/g)	C_e (mg/L)	q_e (mg/g)	C_e (mg/L)	q_e (mg/g)
0	0	0	0	0	0	0	0	0
10	1.081692	0.89183	0	0	1.750982	0.82490	1.6328	0.836712
20	1.396653	1.86033	1.30807	0.86919	2.06594	1.79340	2.833661	1.716633
30	1.987204	2.80126	1.947834	1.805215	3.28641	2.67138	4.09350	2.590646
40	3.138779	3.686122	3.06003	2.693993	4.792322	3.52076	5.94389	3.405610
50	4.260826	4.57391	4.152559	3.584794	5.461614	4.453838	7.636814	4.236318
60	4.783464	5.52165	5.018700	4.498121	7.96161	5.203838	9.861220	5.0138
70	7.75492	6.224507	7.686023	5.231398	10.80612	5.919389	12.00688	5.799311
80	9.615157	7.038482	9.723425	6.02765	13.1092	6.689074	14.64468	6.535531
90	12.23326	7.776628	11.88484	6.811515	14.33956	7.56604	16.00295	7.39970
100	13.42421	8.65757	13.3159	7.668405	16.04232	8.39576	17.83366	8.216633

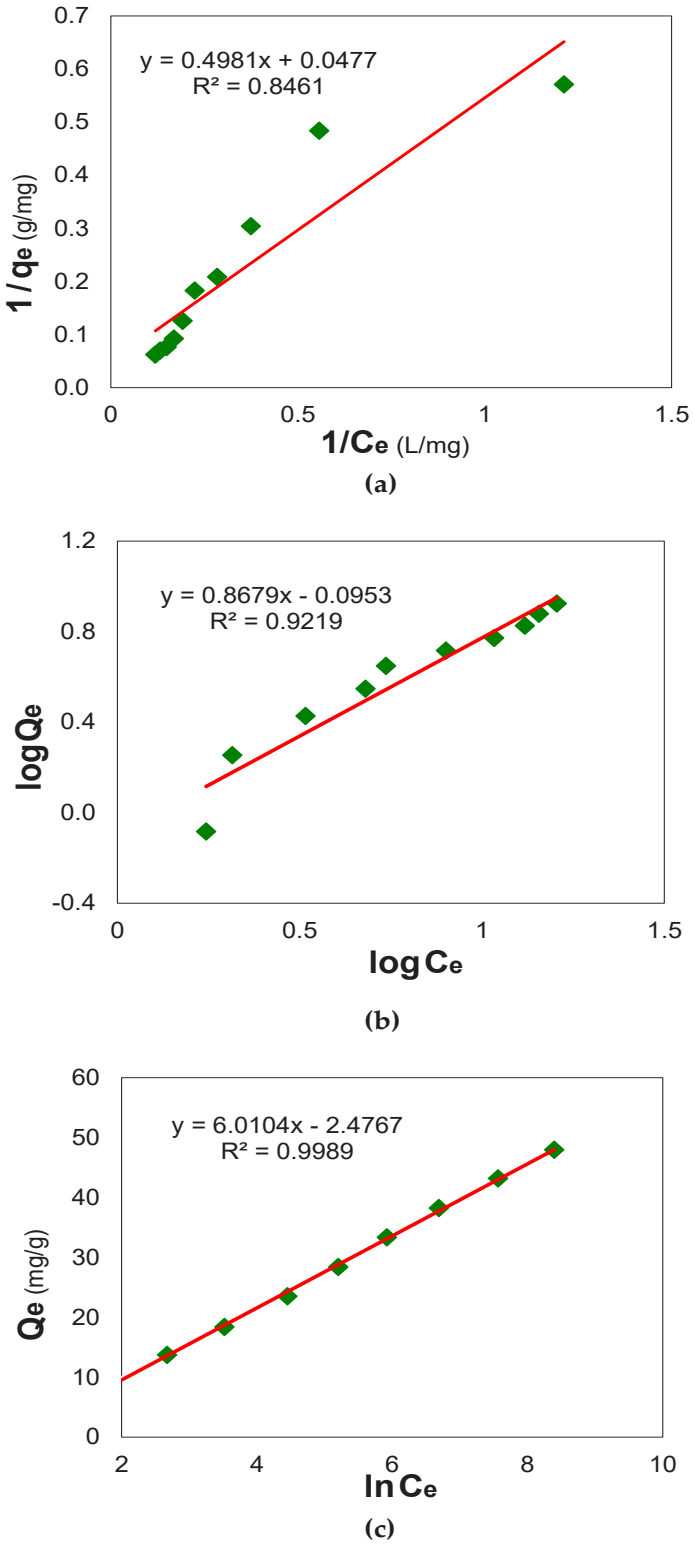

Fig. 7. Plot of (a) Langmuir, (b) Freundlich and (c) Temkin isotherm model for adsorption of Azure C dye onto prepared GO/P(CMC-Co-Am) nanocomposite.

and filling of the porous structure following dye interaction [11].

Isothermal and thermodynamic study

The adsorption of Azur C dye at varying temperatures (10°C, 15°C, 20°C, and 30°C), Fig. 6 and Table 1, shows that the adsorption capacity (Q_e) decreases as the temperature increases. At 10°C, the highest adsorption capacity is observed, with Q_e reaching approximately 8.6 mg/g as the equilibrium concentration (C_e) increases, while at 30°C, the adsorption capacity is the lowest, reaching around 8.2 mg/g. This trend suggests that the adsorption of Azur C dye onto the GO/P(CMC-Co-Am) nanocomposite is an exothermic process, where lower temperatures favor higher adsorption. The decrease in adsorption capacity with increasing temperature may be due to reduced attractive forces between the dye molecules and the adsorbent surface at higher temperatures, or due to the increased kinetic energy of the dye molecules, leading to desorption [54].

The adsorption of Azur C dye onto the GO/P(CMC-Co-Am) nanocomposite was evaluated using the Langmuir isotherm model (Fig. 7a). The linear plot between $1/Q_e$ (inverse of adsorption

Table 2. Parameters calculated from Langmuir, Freundlich and Temkin isotherm model.

Langmuir	Freundlich	Temkin
q_0 (mg/ g)	K_f (mg g^{-1} (mg $L^{-1})^{-1/n}$)	B (J/mol)
20.96	7.377	-2.4766
b (L/g)	n	A_T (L/g)
0.0956	0.503	0.0883
	R^2	
0.8461	0.936	0.9035

Table 3. Effect of temperature for adsorption of Azure C dye onto prepared GO/P(CMC-Co-Am) nanocomposite in terms of equilibrium adsorption capacity (q_e (mg/g)).

Temperature (°C)	q_e (mg/g)
10	8.657579
15	8.447933
20	8.395768
30	8.216634

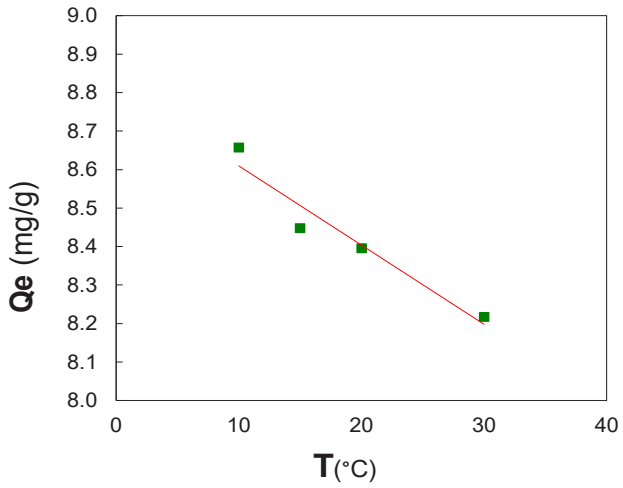

Fig. 8. Effect of temperature for adsorption of Azure C dye onto prepared GO/P(CMC-Co-Am) nanocomposite.

Table 4. Calculated thermodynamic parameters from Van't Hoff plot.

T (°C)	ΔG (kJ/mol)	ΔH (kJ/mol)	ΔS (J/mol K)	K_c
20	1.577	-11.186	-43.496	0.523

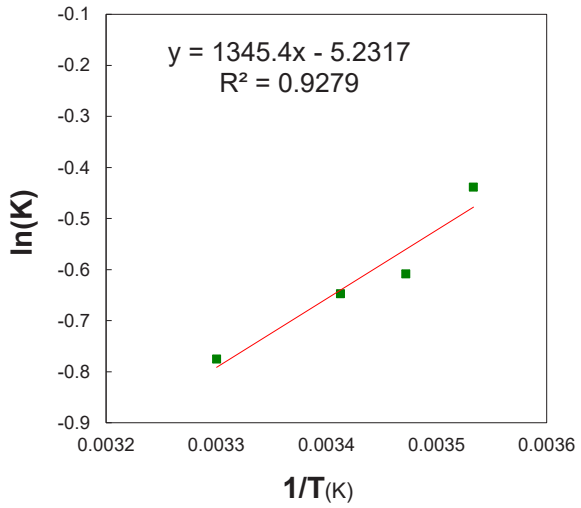

Fig. 9. Van't Hoff plot.

capacity) and $1/C_e$ (inverse of equilibrium concentration) with an R^2 value of 0.8461 suggests that the Langmuir model reasonably describes the adsorption data. The slope and intercept of the plot indicate monolayer adsorption on a homogeneous surface with a finite number of adsorption sites. The Freundlich model, as illustrated in Fig. 7b, shows a positive correlation between the amount of dye adsorbed and its concentration, suggesting heterogeneous adsorption. The R^2 value (0.9219) confirms its suitability for describing this process. In contrast, the Langmuir model assumes monolayer adsorption with a saturation point. Additionally, the Freundlich model, while exhibiting a strong correlation with the adsorption data, may also incorporate some aspects of the Temkin model (with an R^2 value of 0.9989 as outlined in Fig. 7c), suggesting that both heterogeneous adsorption and molecular interactions are involved in the adsorption process of Azure C dye. The comparative analysis of all investigated isotherm models is summarized in Table 2, emphasizing the superior fit of the Freundlich model with a maximum adsorption capacity (qe) of 7.37 mg/g [54].

The effect of temperature presented in Table 3 and Fig. 8 illustrate a slight decrease in adsorption with increasing temperature, suggesting an exothermic process. This indicates that the adsorption process releases heat, which is consistent with the formation of weaker physical bonds or the breaking of chemical bonds between the adsorbate and the adsorbent at higher temperatures. This phenomenon is often observed in physical adsorption, where the interactions between the adsorbate and adsorbent are based on weak intermolecular forces, such as van der Waals forces or dipole-dipole interactions [54].

The thermodynamic data reveals that the adsorption process of Azure C dye is exothermic, meaning it releases heat, and spontaneous at 20°C, indicating that it occurs without external energy input (Table 4). Additionally, the process leads to a decrease in entropy, suggesting that the system becomes more ordered as the dye molecules bind to the adsorbent surface. The high R^2 value of 0.9279 in the Arrhenius plot (Fig. 9) confirms the suitability of the Arrhenius equation in describing the temperature dependence of the adsorption process. This equation relates the rate constant of the process to its activation energy and temperature [55].

CONCLUSION

The GO/P(CMC-Co-Am) nanocomposite effectively adsorbed Azure C dye from aqueous

solutions. Adsorption capacity was temperature-dependent, with optimal performance at lower temperatures, confirming an exothermic process. The Freundlich isotherm best described the adsorption data, suggesting a complex interaction. Thermodynamic parameters indicated a spontaneous and feasible process at room temperature, leading to a more organized system. This research highlights the potential of the GO/P(CMC-Co-Am) nanocomposite as a sustainable and efficient solution for wastewater dye removal, warranting further investigation of its long-term stability and reusability.

CONFLICT OF INTEREST

The authors declare that there is no conflict of interests regarding the publication of this manuscript.

REFERENCES

1. Sahoo C, Gupta AK, Sasidharan Pillai IM. Photocatalytic degradation of methylene blue dye from aqueous solution using silver ion-doped TiO_2 and its application to the degradation of real textile wastewater. Journal of Environmental Science and Health, Part A. 2012;47(10):1428-1438.
2. Khandegar V, Saroha AK. Electrocoagulation for the treatment of textile industry effluent – A review. J Environ Manage. 2013;128:949-963.
3. Rahmani M, Kaykhaii M, Sasani M. Application of Taguchi L16 design method for comparative study of ability of 3A zeolite in removal of Rhodamine B and Malachite green from environmental water samples. Spectrochimica Acta Part A: Molecular and Biomolecular Spectroscopy. 2018;188:164-169.
4. Studies on Removal of Methylene Blue Dye from Aqueous Solution by Adsorption Using Low Cost Adsorbent. Knowledge of Research. 2016.
5. Ibrahim HK, Albo Hay Allah MA, Al-Da'amy MA, Kareem ET, Abdulridha AA. Adsorption of Basic Dye Using Environmental friendly adsorbent. IOP Conference Series: Materials Science and Engineering. 2020;871(1):012027.
6. De Gisi S, Lofrano G, Grassi M, Notarnicola M. Characteristics and adsorption capacities of low-cost sorbents for wastewater treatment: A review. Sustainable Materials and Technologies. 2016;9:10-40.
7. Batool M, Javed T, Wasim M, Zafar S, Din MI. Exploring the usability of Cedrus deodara sawdust for decontamination of wastewater containing crystal violet dye. Desalination and Water Treatment. 2021;224:433-448.
8. Ghzal Q, Javed T, Batool M. Potential of easily prepared low-cost rice husk biochar and burnt clay composite for the removal of methylene blue dye from contaminated water. Environmental Science: Water Research and Technology. 2023;9(11):2925-2941.
9. Shah A, Arjunan A, Thumma A, Zakharova J, Bolarinwa T, Devi S, et al. Adsorptive removal of arsenic from drinking water using KOH-modified sewage sludge-derived biochar. Cleaner Water. 2024;2:100022.
10. Shah A, Zakharova J, Batool M, Coley MP, Arjunan A, Hawkins AJ, et al. Removal of cadmium and zinc from water using sewage sludge-derived biochar. Sustainable Chemistry for the Environment. 2024;6:100118.
11. Mannan HA, Nadeem R, Bibi S, Javed T, Javed I, Nazir A, et al. Mesoporous activated TiO_2 /based biochar synthesized from fish scales as a proficient adsorbent for deracination of heavy metals from industrial efflux. J Dispersion Sci Technol. 2022;45(2):329-341.
12. Majeed HJ, Idrees TJ, Mahdi MA, Abed MJ, Batool M, Yousefi SR, et al. Synthesis and application of novel sodium carboxy methyl cellulose-g-poly acrylic acid carbon dots hydrogel nanocomposite (NaCMC-g-PAAc/ CDs) for adsorptive removal of malachite green dye. Desalination and Water Treatment. 2024;320:100822.
13. Arshad R, Javed T, Thumma A. Exploring the efficiency of sodium alginate beads and Cedrus deodara sawdust for adsorptive removal of crystal violet dye. J Dispersion Sci Technol. 2023;45(12):2330-2343.
14. Javed T, Thumma A, Uddin AN, Akhter R, Babar Taj M, Zafar S, et al. Batch adsorption study of Congo Red dye using unmodified Azadirachta indica leaves: isotherms and kinetics. Water Practice and Technology. 2024;19(2):546-566.
15. Rehman H, Javed T, Thumma A, Uddin AN, Singh N, Baig MM, et al. Potential of easily available low-cost raw cotton for the elimination of methylene blue dye from polluted water. Desalination and Water Treatment. 2024;318:100319.
16. Bukhari A, Javed T, Haider MN. Adsorptive exclusion of crystal violet dye from wastewater by using fish scales as an adsorbent. J Dispersion Sci Technol. 2022;44(11):2081-2092.
17. Imran MS, Javed T, Areej I, Haider MN. Sequestration of crystal violet dye from wastewater using low-cost coconut husk as a potential adsorbent. Water Sci Technol. 2022;85(8):2295-2317.
18. Urooj H, Javed T, Taj MB, Nouman Haider M. Adsorption of crystal violet dye from wastewater on Phyllanthus emblica fruit (PEF) powder: kinetic and thermodynamic. Int J Environ Anal Chem. 2023:1-26.
19. Atyaa AI, Jasim LS, Jamel HO, Sahib IJ. Adsorption of the crystal violet from aqueous solutions on (BIAPEHB/P(AA-co-AM)) composite: Thermodynamic study. AIP Conference Proceedings: AIP Publishing; 2023. p. 040139.
20. Brown P, Atly Jefcoat I, Parrish D, Gill S, Graham E. Evaluation of the adsorptive capacity of peanut hull pellets for heavy metals in solution. Adv Environ Res. 2000;4(1):19-29.
21. Kinetic, Thermodynamic, Equilibrium and Isotherm Studies for the Removal of Methyl Red Dye from Aqueous Solution by Using Low Cost Adsorbent. Journal of Xidian University. 2020;14(9).
22. Wang S, Ning H, Hu N, Huang K, Weng S, Wu X, et al. Preparation and characterization of graphene oxide/silk fibroin hybrid aerogel for dye and heavy metal adsorption. Composites Part B: Engineering. 2019;163:716-722.
23. Wanyonyi WC, Onyari JM, Shiundu PM. Adsorption of Congo Red Dye from Aqueous Solutions Using Roots of Eichhornia Crassipes: Kinetic and Equilibrium Studies. Energy Procedia. 2014;50:862-869.
24. Wekoye JN, Wanyonyi WC, Wangila PT, Tonui MK. Kinetic and equilibrium studies of Congo red dye adsorption on cabbage waste powder. Environmental Chemistry and Ecotoxicology. 2020;2:24-31.
25. Yang J, Wang K, Lv Z, Li W, Luo K, Cao Z. Facile Preparation and Dye Adsorption Performance of Poly(N-isopropylacrylamide-co-acrylic acid)/Molybdenum Disulfide Composite Hydrogels. ACS omega. 2021;6(42):28285-28296.
26. Yuan Z, Wang J, Wang Y, Liu Q, Zhong Y, Wang Y, et al. Preparation of a poly(acrylic acid) based hydrogel with

fast adsorption rate and high adsorption capacity for the removal of cationic dyes. RSC advances. 2019;9(37):21075-21085.
27. Yusuff AS. Adsorption of cationic dye from aqueous solution using composite chicken eggshell - anthill clay: optimization of adsorbent preparation conditions. Acta Polytechnica. 2019;59(2):192-202.
28. Zauro SA, Vishalakshi B. Amphoteric gellan gum-based terpolymer–montmorillonite composite: synthesis, swelling, and dye adsorption studies. International Journal of Industrial Chemistry. 2017;8(3):345-362.
29. Zein R, Tomi ZB, Fauzia S, Zilfa Z. Modification of rice husk silica with bovine serum albumin (BSA) for improvement in adsorption of metanil yellow dye. Journal of the Iranian Chemical Society. 2020;17(10):2599-2612.
30. Zhang J, Li F, Sun Q. Rapid and selective adsorption of cationic dyes by a unique metal-organic framework with decorated pore surface. Appl Surf Sci. 2018;440:1219-1226.
31. Mhammed Alzayd AA, Radia ND. A Novel Eco-friendly Bionanocomposite: Synthesis, Optimizing Grafting Factors, Characterization, Adsorption of Ofloxacin Hydrochloride, Reinforcement Elimination System to Pharmaceutical Contaminants. Journal of Polymers and the Environment. 2023;32(4):1821-1836.
32. Alwan AS, Jasim LS, Sahib IJ. Synthesis and characterization of graphene oxide-(carboxymethylcellulose-sodium alginate - Acrylic acid) hydrogel composite for Azure B removal from aqueous solutions. AIP Conference Proceedings: AIP Publishing; 2023. p. 040001.
33. Al-Hayder LSJ, Al-Hussainawy Mk. Drug Carriers in The Delivery and Release of Hydroxychloroquine by Biopolymer. Research Square Platform LLC; 2023.
34. Alzayd AAM, Radia ND. Novel pH-sensitive of organic composite (kc-g-poly(AAc-co-AAm)/bentonite), synthesis and characterization candidate as a carrier for controlled release system in vitro to some drugs. Carbon Letters. 2024;34(1):505-517.
35. Jiang H, Yang Y, Lin Z, Zhao B, Wang J, Xie J, et al. Preparation of a novel bio-adsorbent of sodium alginate grafted polyacrylamide/graphene oxide hydrogel for the adsorption of heavy metal ion. Sci Total Environ. 2020;744:140653.
36. Rafak SH, Jasim LS. Synthesis of novel bentonite/pectin-grafted-poly(crotonic acid-co-acrylic acid) hydrogel nanocomposite for adsorptive removal of safranin O dye from aqueous solution. Int J Environ Anal Chem. 2024:1-24.
37. Verma A, Thakur S, Mamba G, Prateek, Gupta RK, Thakur P, et al. Graphite modified sodium alginate hydrogel composite for efficient removal of malachite green dye. Int J Biol Macromol. 2020;148:1130-1139.
38. Mohammadzadeh Pakdel P, Peighambardoust SJ, Arsalani N, Aghdasinia H. Safranin-O cationic dye removal from wastewater using carboxymethyl cellulose-grafted-poly(acrylic acid-co-itaconic acid) nanocomposite hydrogel. Environ Res. 2022;212:113201.
39. Zhang H, Liu X, Tian L, Tang Y, Shi Z, Xiao Y, et al. Preparation of Functionalized Graphene Oxide Composite Spheres and Removal of Cu2+ and Pb2+ from Wastewater. Water, Air and Soil Pollution. 2022;233(12).
40. Shah A, Arjunan A, Manning G, Zakharova J, Andraulaki I, Batool M. The effect of dose, settling time, shelf life, storage temperature and extractant on Moringa oleifera Lam. protein coagulation efficiency. Environmental Nanotechnology, Monitoring and Management. 2024;21:100919.
41. Jiang Z, Han X, Zhao C, Wang S, Tang X. Recent Advance in Biological Responsive Nanomaterials for Biosensing and Molecular Imaging Application. Int J Mol Sci. 2022;23(3):1923.
42. Daffalla SB, Mukhtar H, Shaharun MS. Preparation and characterization of rice husk adsorbents for phenol removal from aqueous systems. PLoS One. 2020;15(12):e0243540-e0243540.
43. Behazin E, Ogunsona E, Rodriguez-Uribe A, Mohanty AK, Misra M, Anyia AO. Mechanical, Chemical, and Physical Properties of Wood and Perennial Grass Biochars for Possible Composite Application. BioResources. 2015;11(1).
44. Batool M, Haider MN, Javed T. Applications of Spectroscopic Techniques for Characterization of Polymer Nanocomposite: A Review. Journal of Inorganic and Organometallic Polymers and Materials. 2022;32(12):4478-4503.
45. Azhar-ul-Haq M, Javed T, Abid MA, Masood HT, Muslim N. Adsorptive removal of hazardous crystal violet dye onto banana peel powder: equilibrium, kinetic and thermodynamic studies. J Dispersion Sci Technol. 2022:1-16.
46. Moussa I, Khiari R, Moussa A, Belgacem MN, Mhenni MF. Preparation and Characterization of Carboxymethyl Cellulose with a High Degree of Substitution from Agricultural Wastes. Fibers and Polymers. 2019;20(5):933-943.
47. Leshaf A, Ziani Cherif H, Benmansour K. Adsorption of Acidol Red 2BE-NW Dye from Aqueous Solutions on Carboxymethyl Cellulose/Organo-Bentonite Composite: Characterization, Kinetic and Thermodynamic Studies. Journal of Polymers and the Environment. 2019;27(5):1054-1064.
48. Razavi FS, Mahdi MA, Ghanbari D, Dawi EA, Abed MJ, Ganduh SH, et al. Fabrication and design of four-component $B_{i2}S_3$/$CuFe_2O_4$/CuO/Cu_2O nanocomposite as new active materials for high performance electrochemical hydrogen storage application. Journal of Energy Storage. 2024;94:112493.
49. Kareem NS, Mohammed SA, Abed MJ, Aneed AH, Kamal HM, Zahid NI, et al. New macrocycles incorporating glycolipids via copper-catalyzed triazole coupling. J Carbohydr Chem. 2022;41(1):1-17.
50. Bayati-Komitaki N, Ganduh SH, Alzaidy AH, Salavati-Niasari M. A comprehensive review of Co3O nanostructures in cancer: Synthesis, characterization, reactive oxygen species mechanisms, and therapeutic applications. Biomedicine and Pharmacotherapy. 2024;180:117457.
51. Yasir AF, Jamel HO. Synthesis of a New DPTYEAP Ligand and Its Complexes with Their Assessments on Physical Properties, Antioxidant, and Biological Potential to Treat Breast Cancer. Indonesian Journal of Chemistry. 2023;23(3):796.
52. Awad MA, Jasim Al-Hayder LS. Removel of a Bsoprolol drug from Aqueous Solutions onto Graphene Oxide/ Carboymethyl cellulose sodium / Acryl acid polymer Composite by Adsorption. IOP Conference Series: Materials Science and Engineering. 2020;928(5):052033.
53. Pang YL, Tee SF, Limg S, Abdullah AZ, Ong HC, Wu C-H, et al. Enhancement of photocatalytic degradation of organic dyes using ZnO decorated on reduced graphene oxide (rGO). Desalination and Water Treatment. 2018;108:311-321.
54. Pulat M, Çetin M. Pantoprazole-Na Release from Poly(acrylamide-co-crotonic acid) and Poly(acrylic acid-co-crotonic acid) Hydrogels. Journal of Bioactive and Compatible Polymers. 2008;23(4):305-318.
55. Gopal V, Elango KP. Equilibrium, kinetic and thermodynamic studies of adsorption of fluoride onto plaster of Paris. J Hazard Mater. 2007;141(1):98-105.